Radiation Tolerance of $GaAs_{1-x}Sb_x$ Solar Cells

Hadi Ashfari[1], Brandon K. Durant[1], Tristan Thrasher[1], Logan Abshire[1], Vincent R. Whiteside[1], Shun Chan[2], Dongyoung Kim[2], Sabina Hatch[2], Mingchu Tang[2], Jeremiah S. McNatt[4], Huiyun Liu[2], Martha R. McCartney[3], David J. Smith[3], and Ian R. Sellers[1]

[1] *Department of Physics & Astronomy, University of Oklahoma, Norman, Oklahoma 73019, USA*

[2] *Department of Electrical & Electronic Engineering, University College London, London WC1E, U. K.*

[3]*Department of Physics, Arizona State University, Tempe, Arizona 85287, USA*

[4]*NASA Glenn Research Center, Cleveland, Ohio 44135, USA*

Abstract — High radiation tolerance of $GaAs_{1-x}Sb_x$ -based solar cells is demonstrated for the low-intensity-low-temperature (LILT) conditions of the target planets Saturn, Jupiter, and Mars. The $GaAs_{1-x}Sb_x$-based cells are irradiated with high energy electrons to assess the effect of harsh radiation environment on the solar cell and the response of the cell is then investigated in terms of its photovoltaic operation. This system shows significant radiation resistance to high energy electron environment at the conditions of the planets of interest. An unusual increase of the short circuit current after irradiation is observed at low temperature, which is supported by a simultaneous increase in the external quantum efficiency of the cell under the same conditions. The open circuit voltage and fill factor of the cell are especially tolerant to irradiation, which is also reflected in unchanged dark current-voltage characteristics of the solar cell upon irradiation particularly at LILT.

***Index Terms* — GaAsSb, LILT, Radiation tolerance, solar cells, space application**

I. INTRODUCTION

High efficiency and radiation tolerance are two essential factors required for solar cells working in space. While III-V multi-junction solar cells are used almost ubiquitously in space [1-4], the radiation tolerance of such systems, particularly in deep space brings added complexity to their design since there is large variability in the sub-cell radiation tolerance [5-7]. Although numerous studies have been performed to improve radiation resistance of the tandem structures [8-11], thick cover glass is inevitably required, which increases weight and reduces the specific system power. Although GaAs has now reached record power conversion efficiency levels, its response to high radiation levels under LILT conditions is concerning (particularly around Jupiter and its moons), requiring very thick cover glass, which removes the ability for compact stowage and deployment [8]. Recently, ultrathin GaAs has been shown to offer potential as a more radiation-hard system for space [12], if appropriate optical management can be designed to improve the absorption.

The potential of $GaAs_{1-x}Sb_x$ as a candidate absorber for deployable systems for outer planetary astrobiology CubeSAT and SmallSAT [13] missions is of particular interest. These small satellites have by nature limited area for surface mounted cells that limits the absolute power available. This can be particularly problematic under the *low-intensity-low-temperature* (LILT) conditions in deeper space. Recently, *thin film* CIGS and perovskite, as well as tandem perovskite/CIGS solar cells have all been assessed for such applications in space [14-17]. Optically *thick* optimized $GaAs_{0.86}Sb_{0.14}$ shows remarkable radiation-tolerant performance without encapsulation suggesting this material should be further considered for hostile space missions including those to Jupiter [18] or, for example, in satellite applications in Highly Eccentric Orbits (HEO) that are being considered to provide better internet coverage and navigation accuracy, which require more robust systems than are currently available.

II. EXPERIMENTAL DETAILS

A $GaAs_{1-x}Sb_x$ based p-i-n solar cell was grown using solid source molecular beam epitaxy on n^+-GaAs (100) substrates. An n-type (2×10^{17} cm^{-3}) strain-balanced $GaAs_{1-x}Sb_x$ was grown at 510˚C followed by a 30 nm n-AlGaAsSb back-surface-field (BSF) layer doped with silicon at 2×10^{18} cm^{-3}. This buffer layer was followed by the 1000 nm base region of n-type $GaAs_{0.86}Sb_{0.14}$ and 500 nm of nominally undoped $GaAs_{0.86}Sb_{0.14}$. The initial n-type $GaAs_{1-x}Sb_x$ layer was grown in four 100 nm graded increments ranging from x = 0.08 to 0.14, to 0.19, and then decreased once more to 0.14 to provide strain compensation and to balance the mismatch in lattice constant between GaAs and $GaAs_{1-x}Sb_x$, and therefore achieve high quality material in the active region of $GaAs_{0.86}Sb_{0.14}$. Without such strain management significant defect formation occurs, which is prohibitive to high PV performance [19, 20]. The high optical quality absorber produced using these strain management techniques is illustrated in Figure 1(a), which shows a high-resolution transmission electron microscope (HR-TEM) image that demonstrates the significant absence of defects other than at the lower interfaces of the structure, well away from the active region. An 150 nm Be-doped p-type $GaAs_{0.86}Sb_{0.14}$ emitter (1×10^{18} cm^{-3}), 30 nm p-type AlGaAsSb window layer (1×10^{18} cm^{-3}), and a final 20 nm p^+-$GaAs_{0.86}Sb_{0.14}$ cap layer completed the design of the p-i-n structure.

Devices were fabricated using conventional wet-etching techniques and optical lithography into mesa diodes of average area ~ 0.25 cm^2. The contacts were deposited using thermal evaporation with a Zn-Au grid pattern and a Ni-Ge-Au layer used for the upper p-type and lower n-type contacts, respectively. The samples were annealed at 400˚C for 60 s to facilitate the formation of good ohmic contacts [19-21].

Temperature dependent photoluminescence (PL) was measured in a Janis closed-cycle cryostat between 4.2 K and 300 K using HeNe laser excitation at 632.8 nm, dispersed with a Princeton Instruments spectrometer, and detected using a LN_2 cooled InGaAs linear array. Solar cell current density-voltage (*J-V*) analysis was performed using a Newport Class ABA solar simulator at both 1-sun AM0 and under LILT conditions consistent with Saturn (100 K, 0.01 suns), Jupiter (135 K, 0.037 suns), and Mars (263 K, 0.43 suns), which were referenced to a calibrated Si solar cell. To achieve the LILT conditions of these target planets, the (AM0) illumination intensity was controlled via a system of fine mesh grids, which allowed adjustment of the light level without effecting the spectrum of the source [22].

External Quantum Efficiency (EQE) measurements were performed using a custom-built current preamplifier based on a Stanford Research Systems SR555. The chopped signal was collected with a Stanford Research Systems SR830 Lock-in amplifier. A quartz-tungsten-halogen (QTH) lamp was used as the light source, and the reference spectrum was collected via calibrated Ge and Si photodiodes. Temperature control was provided for both the *J-V* and EQE measurements by a Linkam cryostat cooled with LN_2 in an evacuated sample chamber. To mimic the exposure of the solar cells to space conditions, each was exposed to 1-MeV electron irradiation at a fluence of 1×10^{15} electrons/cm^2, which fully penetrated the active region of the structure. Irradiation was conducted at the NEO Beam facility in Ohio, and the fluence was monitored with a Faraday cup and CTA film. Cross section observations were made using an image-corrected Titan 80-300 transmission electron microscope (TEM) operated at 300 kV.

III. RESULTS AND DISCUSSION

The structure of the GaAsSb-based solar cell is shown in the TEM image of the cross section of the cell layers in Figure 1(a). Strips of the high-energy AlGaAsSb window layers clearly stand out with lighter contrast in the TEM image. Strain relaxation via defect generation is visible in the lower parts of the cell between the substrate and the BSF but no defects are visible in the upper layers. Figure 1(b) shows the

energy band offsets simulated for this device using NRL Bands© and indicates preferential band alignments for minority carrier extraction in this structure.

Figure 1(c) shows External Quantum Efficiency (EQE) and Photoluminescence (PL) response of the solar cell at room temperature. The band gap energy of the material is reflected in the peak of the PL, which is well matched to the absorption edge of the EQE response at ~ 1100 nm (1.12 eV). This peak in the EQE at ~ 700 nm reflects the absorption in the AlGaAsSb window layer. Some evidence of lower energy defect or impurities states is observed in the PL, which is attributed to unintentional alloy fluctuations and the background impurity concentration in this doped structure.

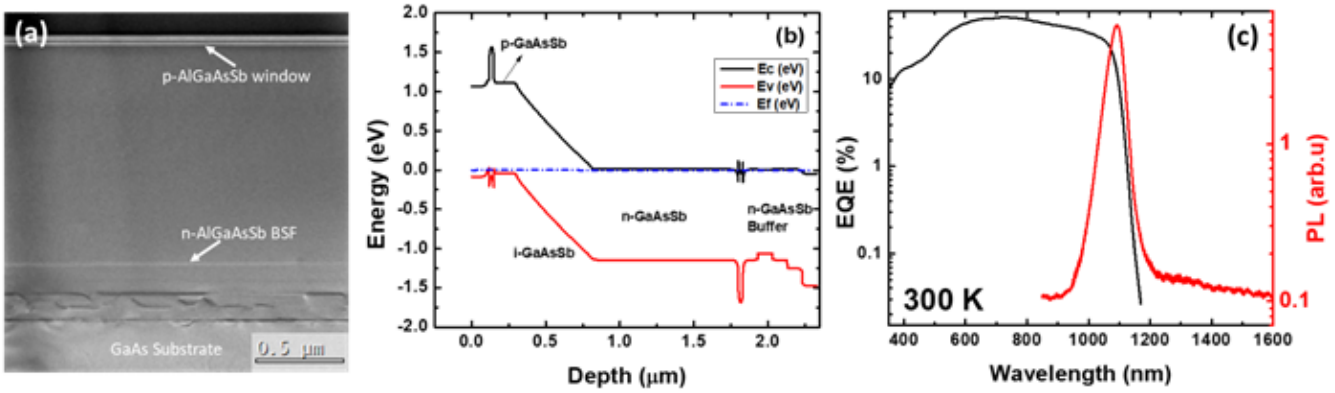

Figure 1: (a) TEM cross section showing the cell layers, (b) Simulated energy band alignments for the structure calculated using NRL Bands illustrating the relative positions of the conduction (E_c) and valence band (E_v), in addition to the Fermi-level (E_f) at equilibrium. (c) EQE and PL response of the solar cell at 300 K. Right axis in red shows the PL response and left axis in black shows the EQE response.

Figure 2(a) shows the temperature-dependent PL of the solar cell from 4.2 to 300 K prior to electron irradiation. At low temperature (T < 80 K), the PL is dominated by a low energy shoulder (1075 nm), which persists until ~ 200 K. With increasing temperature, the dominant peak evolves and a second higher energy transition emerges at ~ 1010 nm (4.2 K), which dominates at T > 80 K. This higher energy peak is attributed to the fundamental band gap of the $GaAs_{0.86}Sb_{0.14}$, which shifts to longer wavelength with increasing temperature following a Varshni-type dependence [23]. The apparent dominance of a lower energy transition and the subsequent thermal redistribution of carriers into the higher energy band gap is well known in III-V ternaries/quaternaries such as GaInNAs [24, 25], AlInAs [26], and InAlAsSb [27], and is generally attributed to carriers trapped in shallow potential and/or alloy fluctuations.

Similar effects were also recently seen in $GaAs_{1-x}Sb_x$ material [28] equivalent to that studied here, where the low energy transition was attributed to the presence of localized states due to increasing Sb-segregation. With increasing temperature, the thermal energy of carriers localized in such alloy fluctuations increases, redistributing carriers into the bands of the system reducing the presence of the defect band and reflecting the band gap PL at higher temperatures. Further evidence of this phenomenological description is illustrated in Figure 2(c), which shows the energy dependence of the peak PL position with temperature for these materials before (solid black squares) and after (solid red squares) high energy electron irradiation. These data show the classic s-shape dependence of materials affected by carrier localization and sample inhomogeneity at lower temperatures. Specifically, at low and increasing temperature (4.2 K < T < 100 K) carriers frozen in defect states redistribute to a subset of high density and lower energy impurity states, reducing (or red shifting) the peak PL emission energy. At T > 90-100 K the thermal energy of the carriers

screens the localization energy and the PL blue shifts to that of the band gap energy, thereafter (T > 100 K) following the conventional temperature dependence of the band gap.

Figure 2(b) shows the temperature dependence of the same *unencapsulated* sample after irradiation with 1 MeV electrons at a fluence of ~ 1×10^{15} electrons/cm^2. Such fluences are equivalent to (or exceed) the particularly harsh fluences experienced by PV systems *with* 0.5 mm covered glass around the Jovian moon, *Io* with its harsh volcanic atmosphere, and greater than those at the icy moon, *Europa*; both systems of scientific interest to the space community but prohibitive to current III-V technology without thick and therefore weighty cover glass architectures [18]. Here, the significant radiance tolerance of the GaAsSb solar cells under investigation to 1 MeV electrons without cover glass, suggests that considerably thinner encapsulation would be required in this case – to prevent damage form particularly damaging lower energy particles – and therefore significantly higher specific powers are also possible for GaAsSb based systems.

While the behavior of the sample (after irradiation) is qualitatively similar, there are subtle differences. Firstly, the PL response of the irradiated sample now has a more pronounced feature related to the lower energy peak assigned to localized states, which indicates that irradiation increases density of such states within the absorber. This is expected since irradiation will inevitably introduce defects and disorder to the lattice through displacement of atoms or electron ionization. From the fact that irradiation does not *apparently* create a new defect state but contributes to the existing localized states it can be inferred that electron irradiation advocates the same type of the defects/states that are introduced to the system via increasing the Sb component.

At low temperature, the dominant defect band has a slightly higher energy which is the case for the PL, in general (see Figure 2(c)). Indeed, while the redistribution of carriers is once more evident as a function of temperature in the irradiated sample, the band gap has increased by ~ 8-10 meV. This is more clearly evident in Figure 2(c) at temperatures above 100 K in the free carrier regime. This behavior suggests that the irradiation of the sample has served to relaxed (coherent) strain in the sample, presumably due to electron ionization via the high energy electrons during irradiation of the sample, which results in local heating rather than significant nuclear displacement [29]. While this effect has certainly affected the sample, it does not appear to appreciably increase (or reduce) the contribution of the sub-gap impurity related emission, as is evident in Figure 2(c) where the dependence of the band gap appears to have simply scaled to higher energy upon irradiation. Further evidence of an irradiation-induced change in band gap is observed in Figures 3(b) and (d), which compare the EQE before and after irradiation at 80 K and 300 K, respectively. This is discussed further below.

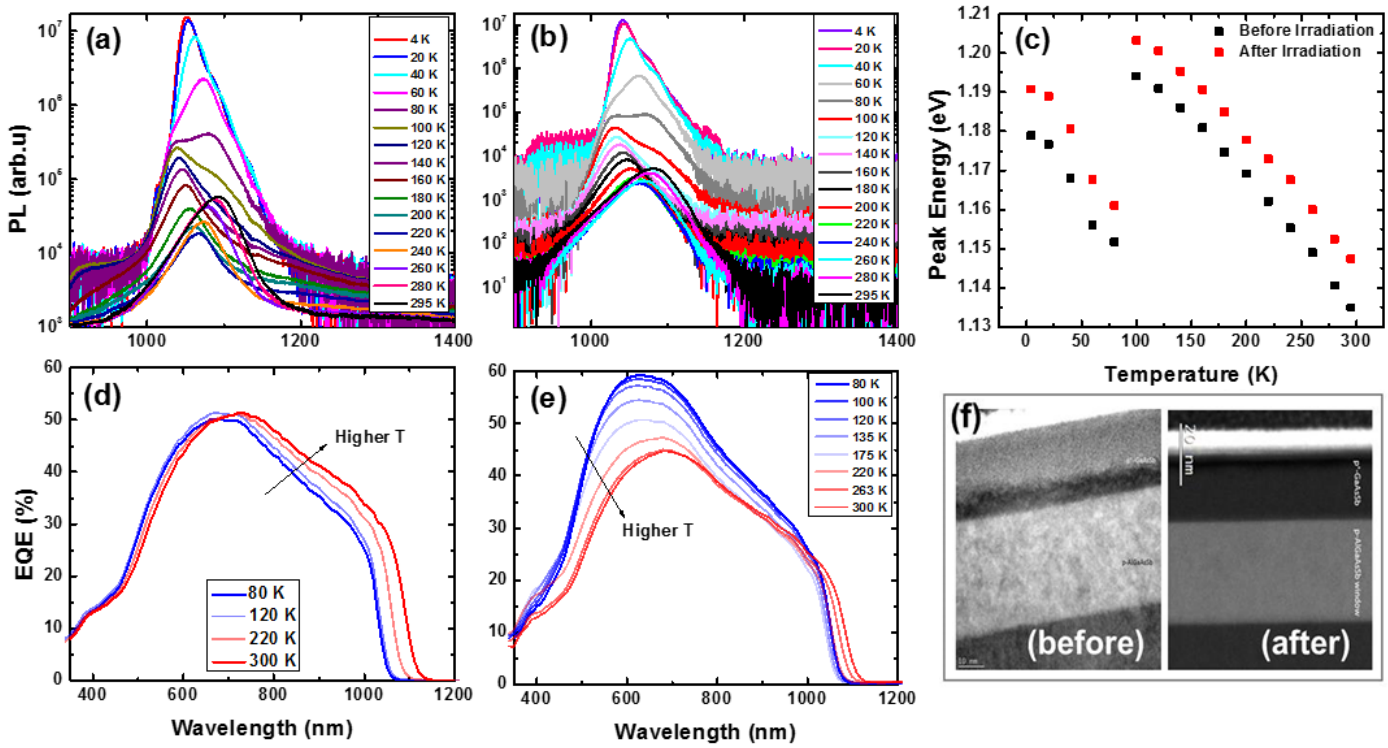

Figure 2: (a) Photoluminescence (PL) of the solar cell as a function of temperature: (a) prior to irradiation, and (b) after exposure to a 1 MeV electrons with a fluence of 1×10 electron/cm^2. (c) Comparison of the peak PL position versus temperature for the pre- (solid black squares) and post- (solid red squares) electron irradiated solar cells as extracted from (a) and (b). EQE behavior of the $GaAs_{1-x}Sb_x$ solar cells as a function of temperature before (d) and (e) after electron irradiation, respectively. (f) HRTEM images of the upper p-AlGaAsSb/p$^+$-GaAsSb interfaces before and after exposure to high-energy electron radiation.

To assess the effects of irradiation upon the device properties temperature dependent EQE measurements were performed before and after exposure to high energy electron irradiation. These data are shown in Figure(s) 2(d) and (e), respectively. When comparing the dependences of the post and pre-irradiated devices it is clear the low temperature (in particular) behavior of the samples is very different after irradiation. The as-grown device (Figure 2(d)) displays a rather typical energy redshift and increasing total EQE with increasing temperature; this is related to the temperature dependence of the $GaAs_{0.86}Sb_{0.14}$ band gap and increasing minority carrier extraction at elevated temperatures, as carriers begin to escape the localization centers at elevated temperatures (as discussed above and evident in the PL – Figure 2(c)).

The electron irradiated sample, however, displays rather unusual properties, which is shown in Figure 2(e). The low temperature EQE for the solar cell exposed to an electron fluence of 1×10^{15} electrons/cm^2 has a *significantly improved* EQE at T < 100 K, with particular improvements in the visible region of the spectrum. As the temperature is increased, the EQE shifts as expected, and the EQE quenches (and more significantly so at higher energy) reaching levels lower than those evident in the unirradiated sample at 300 K. This behavior can be more clearly observed in Figure 3, which shows direct comparisons of the AM0 current-voltage responses and EQE at 80 K and 300 K for the devices before and after irradiation.

Figure 3 (a) compares the light current density-voltage (*J-V*) results before and after irradiation of the $GaAs_{1-x}Sb_x$ based solar cell under AM0 illumination at 80 K. The J_{SC} of the solar cell here after (24.5 mA/cm^2) irradiation (solid red triangles) is greater than that of the pre-irradiated (23.3 mA/cm^2) device

(solid black squares) while there is negligible difference in V_{OC} for the two devices at this temperature (80 K). This behavior is further reflected in Figure 3(b), which compares the EQE of the two solar cells, also at 80 K. While the J_{sc} values extracted from the EQE are lower than those extracted from the *J-V* analysis (Figure 3(a)) due to the lower illumination levels of the EQE measurements relative to the broadband solar irradiation of the solar simulator, the qualitative behavior observed in the EQE is the same, and the large improvement in the EQE at low temperature upon irradiation is very clear in Figure 3(b). Interestingly, the decrease in energy gap evident in the PL *and* here in the EQE upon irradiation is not reflected in any significant reduction in V_{OC} for the irradiated device, indicating no appreciable increase - or significant *additional* contribution - of non-radiative recombination in the irradiated sample, *at low temperatures*. However, it should be noted that the V_{OC} at low (Figure 3(a)) and room temperature (Figure 3(c)) both before and after irradiation, are significantly lower than might be expected for an absorber with a direct band gap of 1100 nm (1.12 eV), which would ideally be closer to 0.7 eV. This loss in V_{OC} is the current limiting factor of these devices, which requires attention before these systems can compete practically in terms of power conversion efficiency with state-of-the-art III-V solar cells. This loss of V_{OC} is attributed to the non-optimum design of the current structure, which was developed predominately to assess the potential to grow thick strain compensated GaAsSb on GaAs. As such, the current proof-of-principle GaAsSb architectures suffer significant recombination losses across the thick intrinsic region due to the alloy fluctuations described above, and the subsequent unintentional high background impurity concentration that result in the absorber of the p-i-n structure.

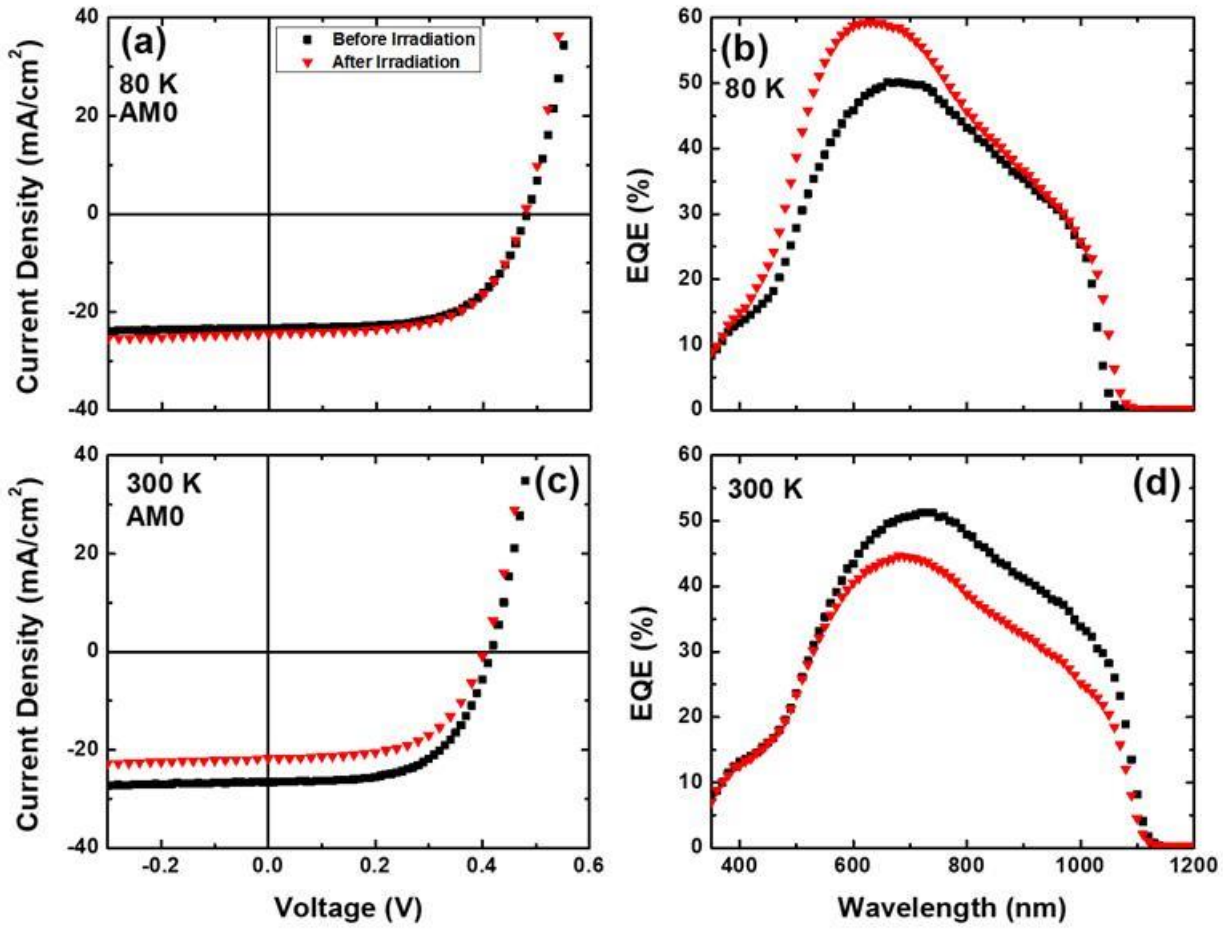

Figure 3: Current density – voltage at AM0 of the $GaAs_{1-x}Sb_x$ solar before (solid black squares) and after (solid red triangles) electron irradiation at (a) 80 K and (c) 300 K. The associated EQE are shown in (b) at 80 K and (d) 300 K.

Comparisons of *J-V* and EQE for the two devices at 300 K are presented in Figures 3(c) and (d), respectively. Contrary to the comparison at 80 K – but consistent with the TD EQE shown in Figures 2(c) and (d) – the relative performance of the pre-irradiated sample (solid black squares) now out-performs the irradiated solar cell (solid red triangles), as might be expected. This unusual behavior in the blue region of the solar spectrum at low temperatures evident in the TD EQE, and the transition to behavior more consistent with the pre-irradiated sample at 300 K (see Figure(s) 2(e) and (d)) whilst requiring further investigation, appears related to unavoidable local heating (or annealing) of the solar cells upon irradiation. Evidence of this hypothesis is shown in Figure 2(f), which shows HR-TEM of the emitter and cap region of the device before (left) and after (right) high energy electron irradiation. In the pre-exposed samples (before) the upper roughly two-thirds of the n^+-GaAsSb cap is amorphous, presumably due to the large impurity concentration in this layer incorporated during MBE growth.

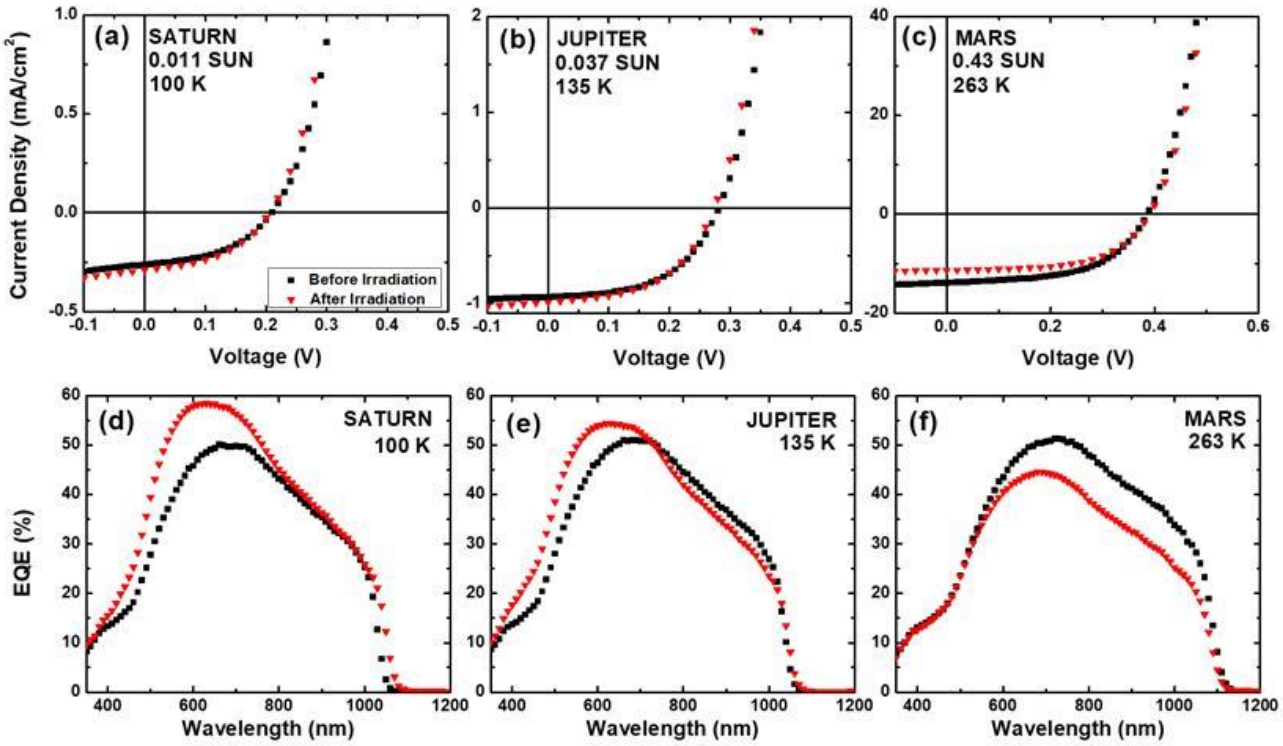

Figure 4: (a) Current Density-Voltage (JV) results at room temperature for before and after irradiation. (b) External Quantum Efficiency (EQE) results at room temperature for before and after irradiation. The solid black squares shows results before irradiation and the solid red line triangles those data after irradiation.

After exposure, the n^+-GaAsSb is highly crystalline indicating some form of annealing and improvement of the layer upon irradiation. Such local heating of the device would indeed be consistent with electron ionization processes when exposed to 1 MeV electrons, which is the primary energy loss mechanism when high energy particles pass through the device, in this case stopping deep in the substrate of the solar cell structure. This improved crystallinity clearly enhances the extraction of carriers at the top of the cell at low temperature. The decrease in performance with increasing temperature is non-trivial and likely relates the ionization of impurities at defect sites and/or interfaces in the emitter region of the structure but, requires further work for a more quantitative interpretation.

To access the potential for GaAsSb-based solar cells for outer planetary missions, the devices were studied in the LILT conditions governing the outer planetary objects of Saturn, Jupiter, and Mars. The data for these

three planets are shown in Figure 4. When considering the *J-V* for the lower temperature Saturn (100 K) and Jupiter (135 K) environments shown in Figure(s) 4(a) and (b), respectively, only small changes are observed in the pre- and post-irradiated solar cells. Interestingly, these small differences are reflected in the irradiated solar cells as slightly higher J_{SC} under the conditions of Saturn, which changes from 0.26 mA/cm^2 before, to 0.29 mA/cm^2 after irradiation, and at Jupiter from 0.93 mA/cm^2 to 0.99 mA.cm^2 upon irradiation, while the V_{OC} is reduced only marginally in these cases. In the case of Mars, with its higher temperature (263 K) and intensity (see Figure 4(c)), the V_{OC} is unchanged, while J_{SC} is reduced from 13.8 mA/cm^2 to 11.3 mA/cm^2 upon electron irradiation. The smaller relative J_{sc} values at Saturn (0.011 sun) with respect to Jupiter (0.037 sun), and then Mars (0.43 sun), simply reflects the increasing solar irradiance experienced by the planetary objects that are closer to the sun. Practically, this results in an adjusted AM0 spectrum at these different distances. The relative contributions of which are indicated in the brackets above, and for the respective planets in Figures 4(a), (b), and (c).

In all cases (Saturn, Jupiter, and Mars), the degradation of the V_{OC} after irradiation is negligible, and all the solar cells show a very high level of radiation tolerance under all the LILT conditions assessed. These data reflect the little influence observed upon the dark *J-V* response upon irradiation (not shown for brevity), and therefore consequently little additional losses associated with non-radiative recombination after irradiation. This unusual behavior is once again tentatively attributed to the effects of electron ionization or local heating of the crystal lattice upon exposure to the 1.0 MeV electron flux, which anneals the sample reducing some of the inhomogeneity and alloy fluctuations known to exist in most quaternaries, particularly mixed group-V Sb [27, 28, 30]. Such annealing is supported by the crystallization of the n^+-GaAsSb cap after exposure, as observed in Figure 2(f).

The EQE of the irradiated solar cells under LILT conditions are shown in Figure(s) 4(d) – (f) for Saturn, Jupiter, and Mars, respectively. These EQE reflect the J_{SC} results acquired in the light *J-V* responses shown in Figure(s) 4(a) – (c), as expected. At the temperature of Saturn and Jupiter, the J_{SC} values produced are higher after irradiation. Accordingly, an increase in the EQE signal is obvious in the entire spectrum for the case of Saturn (d) and particularly at the high energy side of the spectrum in the case of Jupiter (e). However, in the case of Mars there is a reduction in the EQE signal upon irradiation consistent with the J_{SC}, which is above the transition temperature observed in the temperature dependent AM0 EQE shown in Figure 2(e), where impurities or defects in the emitter region appear to be ionized, and where carrier localization is reduced.

The phenomena of increasing J_{SC} (and associated EQE) after irradiation has been reported previously for III-V solar cell structures [12, 31], and more recently in the halide perovskites [29]. These effects have been assigned to carrier removal and changing of the doping profile of layers upon irradiation, which can lead to extension of the depletion region width resulting in enhanced carrier collection under specific circumstances [12, 29, 31]. Here, an improvement in the carrier collection efficiency and expansion of the depletion region width in the absorber can be inferred from higher EQE signals for the high energy part of the spectrum, which extend towards low energy at low temperatures in the irradiated cell. However, in order to better understand the temperature-dependent behavior of these effects, additional irradiated GaAsSb solar cells with varied fluence and energy, along with more temperature-dependent experiments, are needed.

IV. CONCLUSION

The radiation tolerance of $GaAs_{1-x}Sb_x$-based solar cells is investigated under the various LILT conditions of Saturn, Jupiter, and Mars. Remarkably, high radiation resistance is observed in photovoltaic properties of the solar cells *upon irradiation* and high performance is observed particularly with respect to V_{OC} and *FF*.

Moreover, an unusual increase in the J_{SC} of the irradiated devices was observed at low temperature, which was reflected in excellent performance for the solar cells measured in the environments of Saturn and Jupiter. While some loss of performance of the electron irradiated devices was observed at the higher solar irradiance and temperature for Mars, these losses were predominantly in J_{SC}. These unusual effects, particularly at low temperatures, were tentatively attributed to local heating upon electron irradiation, and defect passivation at lower temperatures, followed by impurity ionization and reduced carrier extraction at higher temperature.

ACKNOWLEDGMENTS

The authors acknowledge funding through the State of Oklahoma Center for the Advancement of Science & Technology (OCAST-OARS) Program, Grant No.: AR-18-052, and in the U.K. through the Engineering and Physical Sciences Research Council program EP/P006973/1, EP/K029118, and the National Epitaxy Facility. TT and LA acknowledge summer support at NASA Glenn Research Center through the OK-LSAMP program. MRM and DJS acknowledge use of facilities in the John M. Cowley Center for High Resolution Electron Microscopy at Arizona State University.

REFERENCES

[1] T. Markvart, A. McEvoy, L. Castaner, Practical handbook of photovoltaics: fundamentals and applications, Elsevier, 2003.
[2] S. Kalogirou, McEvoy's handbook of photovoltaics: fundamentals and applications, Academic Press, 2017.
[3] M. Lumb, S. Mack, K. Schmieder, M. González, M. Bennett, D. Scheiman, M. Meitl, B. Fisher, S. Burroughs, K. Lee, J. Rogers, R. Walters, GaSb-Based Solar Cells for Full Solar Spectrum Energy Harvesting, Advanced Energy Materials, 7 (2017) 1700345.
[4] M. Imaizumi, T. Nakamura, T. Takamoto, T. Ohshima, M. Tajima, Radiation degradation characteristics of component subcells in inverted metamorphic triple‐junction solar cells irradiated with electrons and protons, Progress in Photovoltaics: Research and Applications, 25 (2017) 161-174.
[5] J. Parravicini, F. Arcadi, A. Le Donne, R. Campesato, M. Casale, E. Greco, S. Binetti, Effect of the irradiation on optical and electrical properties of triple-junction flexible thin solar cells for space applications, Frontiers in Physics, 7 (2019) 169.
[6] M. Yamaguchi, Radiation-resistant solar cells for space use, Sol. Energy Mater. Sol. Cells, 68 (2001) 31-53.
[7] R.H.v. Leest, D. Fuhrmann, A. Frey, M. Meusel, G. Siefer, S.K. Reichmuth, Recent progress of multi-junction solar cell development for CPV applications at AZUR SPACE, AIP Conference Proceedings, 2149 (2019) 020007. 10.1063/1.5124177
[8] A. Bett, D. Frank, W. Guter, R. Hoheisel, E. Oliva, S. Philipps, J. Schöne, G. Siefer, M. Steiner, A. Wekkeli, E. Welser, M. Meusel, W. Köstler, G. Strobl, Highest efficiency multi-junction solar cell for terrestrial and space applications, 24th European Photovoltaic Solar Energy Conference and Exhibition, (2009).
[9] A. Khan, M. Yamaguchi, N. Dharmaras, T. Yamada, T. Tanabe, S. Takagishi, H. Itoh, T. Ohshima, M. Imaizumi, S. Matsuda, Radiation resistant low bandgap InGaAsP solar cell for multi-junction solar cells, Japanese Journal of Applied Physics, 40 (2001) L728.
[10] P. Colter, B. Hagar, S. Bedair, Tunnel junctions for III-V multijunction solar cells review, Crystals, 8 (2018) 445.
[11] I. Garcia, I. Rey-Stolle, C. Algora, Performance analysis of AlGaAs/GaAs tunnel junctions for ultra-high concentration photovoltaics, Journal of Physics D: Applied Physics, 45 (2012) 045101. 10.1088/0022-3727/45/4/045101
[12] L. Hirst, M. Yakes, J. Warner, M. Bennett, K. Schmieder, R. Walters, P. Jenkins, Intrinsic radiation tolerance of ultra-thin GaAs solar cells, Applied Physics Letters, 109 (2016) 033908.
[13] M. Sweeting, Modern small satellites-changing the economics of space, Proceedings of the IEEE, 106 (2018) 343-361.
[14] C.R. Brown, V.R. Whiteside, D. Poplavskyy, K. Hossain, M.S. Dhoubhadel, I.R. Sellers, Flexible Cu(In,Ga)Se_2 Solar Cells for Outer Planetary Missions: Investigation Under Low-Intensity Low-Temperature Conditions, IEEE Journal of Photovoltaics, 9 (2019) 552-558. 10.1109/JPHOTOV.2018.2889179
[15] H. Afshari, B.K. Durant, C.R. Brown, K. Hossain, D. Poplavskyy, B. Rout, I.R. Sellers, The role of metastability and concentration on the performance of CIGS solar cells under Low-Intensity-Low-Temperature conditions, Sol. Energy Mater. Sol. Cells, 212 (2020) 110571.
[16] C. R. Brown, G. E. Eperon, V. R. Whiteside, I. R. Sellers, Potential of high-stability perovskite solar cells for low-intensity–low-temperature (LILT) outer planetary space missions, ACS Applied Energy Materials, 2 (2018) 814-821.

[17] F. Lang, M. Jošt, K. Frohna, E. Köhnen, A. Al-Ashouri, A.R. Bowman, T. Bertram, A.B. Morales-Vilches, D. Koushik, E.M. Tennyson, Proton Radiation Hardness of Perovskite Tandem Photovoltaics, Joule, (2020).
[18] G.A. Landis, J. Fincannon, Study of power options for Jupiter and outer planet missions, in: 2015 IEEE 42nd Photovoltaic Specialist Conference (PVSC), IEEE, 2015, pp. 1-5.
[19] H. Liu, I. R. Sellers, M. Gutierrez, K. Groom, W. Soong, M. Hopkinson, J. David, R. Beanland, T. Badcock, D. Mowbray, Influences of the spacer layer growth temperature on multilayer InAs ／ GaAs quantum dot structures, Journal of applied physics, 96 (2004) 1988-1992.
[20] I. R. Sellers, H.Y. Liu, T.J. Badcock, D.J. Mowbray, M.S. Skolnick, K. M. Groom, M. Gutierrez, M. Hopkinson, J. S. Ng, J. P. R. David, and R. Beanland, Optimizing the growth of 1.3 μm multi-layer quantum dot lasers using a high-temperature-growth GaAs spacer layers, Appl. Phys. Lett, 85 (2004) 704-706.
[21] F. Tutu, I. R. Sellers, M. Peinado, C. Pastore, S. Willis, A. Watt, T. Wang, H. Liu, Improved performance of multilayer InAs/GaAs quantum-dot solar cells using a high-growth-temperature GaAs spacer layer, in, American Institute of Physics, 2012.
[22] D.A. Scheiman, D.B. Snyder, Low intensity low temperature (LILT) measurements of state-of-the-art triple junction solar cells for space missions, in: 2008 33rd IEEE Photovoltaic Specialists Conference, 2008, pp. 1-6. 10.1109/PVSC.2008.4922707
[23] Y.P. Varshni, Temperature dependence of the energy gap in semiconductors, Physica, 34 (1967) 149-154.
[24] C.R. Brown, N.J. Estes, V.R. Whiteside, B. Wang, K. Hossain, T.D. Golding, M. Leroux, M. Al Khalfioui, J.G. Tischler, C.T. Ellis, E.R. Glaser, I.R. Sellers, The effect and nature of N–H complexes in the control of the dominant photoluminescence transitions in UV-hydrogenated GaInNAs, RSC Advances, 7 (2017) 25353-25361. 10.1039/C7RA02900D
[25] T. Nuytten, M. Hayne, B. Bansal, H.Y. Liu, M. Hopkinson, V.V. Moshchalkov, Charge separation and temperature-induced carrier migration in Ga${}_{1\ensuremath{-}x}$In${}_{x}$N${}_{y}$As${}_{1\ensuremath{-}y}$ multiple quantum wells, Physical Review B, 84 (2011) 045302. 10.1103/PhysRevB.84.045302
[26] H. Esmaielpour, V.R. Whiteside, L. Hirst, J. Tischler, R. Walters, I. R. Sellers, The effect of an InP cap layer on the photoluminescence of an InxGa1 xAsQ yPy/InzAlQ zAs quantum well heterostructure, Journal of Applied Physics, 121 (2017) 235301.
[27] S. Tomasulo, M. Gonzalez, M.P. Lumb, C.R. Brown, A.H. Dicarlo, I.R. Sellers, I. Vurgaftman, J.R. Meyer, R.J. Walters, M.K. Yakes, Effect of molecular beam epitaxy growth conditions on phase separation in wide-bandgap InAlAsSb lattice-matched to InP, Journal of Crystal Growth, 548 (2020) 125826.
[28] X. Gao, Z. Wei, F. Zhao, Y. Yang, R. Chen, X. Fang, J. Tang, D. Fang, D. Wang, R. Li, Investigation of localized states in GaAsSb epilayers grown by molecular beam epitaxy, Scientific reports, 6, 29112 (2016).
[29] B. K. Durant, H. Afshari, S. Singh, B. Rout, G. E. Eperon and I. R. Sellers, Tolerance of Perovskite Solar Cells to Targeted Proton Irradiation and Electronic Ionization Induced Healing, ACS Energy Letters, 6, 2362 (2021).
[30] J. Tang, V.R. Whiteside, H. Esmaielpour, S. Vijeyaragunathan, T. Mishima, M. Santos, I. Sellers, Effects of localization on hot carriers in InAs/AlAsxSb1 x quantum wells, Applied Physics Letters, 106, 061902 (2015).
[31] R. J. Walters, S. Messenger, J.H. Warner, C.D. Cress, M. Gonzalez, S. Maximenko, Modeling of radiation induced defects in space solar cells, in: Physics and Simulation of Optoelectronic Devices XIX, International Society for Optics and Photonics, 2011, pp. 79330P.